Intertwined Analytical, Experimental and Theoretical Studies on the Formation and Structure of a Copper Dienolate

Baptiste Lecachey, Laetitia Palais, Benoît Courcy, Samira Bouauli, Muriel Durandetti, Hassan Oulyadi, Anne Harisson-marchand, Jacques Maddaluno, Hélène Gérard, Emmanuel Vrancken, et al.

Intertwined Analytical, Experimental and Theoretical Studies on the formation and structure of a Copper dienolate.

Baptiste Lecachey, [b] Laetitia Palais,[c] Benoît de Courcy,[a] Samira Bouauli,[a] Muriel Durandetti,*[c] Hassan Oulyadi,*[c] Anne Harisson-Marchand,[c] Jacques Maddaluno,[c] Hélène Gérard,*[a] Emmanuel Vrancken,*[b] and Jean-Marc Campagne*[b]

[a] Dr. Benoit de Courcy, Dr. Samira Bouaouli, Prof. Hélène Gérard
Sorbonne Université, CNRS, Laboratoire de Chimie Théorique, LCT , F-75005 Paris, France.
[b] Dr. Baptiste Lecachey, Prof. Jean-Marc Campagne, Dr. Emmanuel Vrancken
ICGM, Univ. Montpellier, CNRS, ENSCM, Montpellier, France.
[c] Dr. Laetitia Palais, Dr. Muriel Durandetti, Prof. Hassan Oulyadi, Dr. Anne Harisson-Marchand, Dr. Jacques Maddaluno
Normandie Univ., UNIROUEN, INSA Rouen, CNRS, Laboratoire COBRA (UMR 6014 & FR 3038), 76000 Rouen, France

Supporting information for this article is given via a link at the end of the document.

Abstract: The reaction of a silyl dienolate, a Cu(II) salt and TBAT yielding the corresponding copper dienolate is addressed. A combined NMR and cyclic voltammetry analysis first highlight the role of TBAT in the Cu(II) to Cu(I) reduction and the structure of the precatalytic species. From these first results a second set of NMR and theoretical studies enable the determination of the structure and the mechanism of formation of the copper dienolate catalytic species. Finally, we showed that that the copper catalyst promote the *E*/*Z* s-*cis* / s-*trans* equilibration of the silyl dienolate precursor through a copper dienolate intermediate. All of these results unveil some peculiarities of the catalytic and asymmetric vinylogous Mukaiyama reaction.

Introduction

For many years, the real structure of organometallic species in solution has remained unknown thus limiting a fine comprehension of reaction mechanisms. Cutting-edge analytical and DFT techniques could lift a corner of the veil and thus pave the way for new synthetic developments.

Organometallic reagents can be roughly divided in two major classes whether they are subjected or not to metallotropic equilibrium. Due to possible multiple aggregation states and equilibrium between them, the structural determination of organometallic reagents without metallotropic equilibrium is in itself challenging. For organometallics subject to metallotropic equilibrium, the situation is even more complex. Copper enolates, a popular class of organometallic reagents due to their polyfunctionality, belong to this last category. Although copper enolates are commonly used in various synthetic applications such as copper catalyzed reductive-,[1] Mukaiyama-,[2]alkylative-,[3]borylative-,[4] direct-[5] aldol or Mannich or Michael type reactions, little is known about their structure, and the mechanisms of these processes are, to the best of our knowledge, not fully described and understood. Among these reactions, we became interested in the development of copper-catalyzed catalytic and asymmetric vinylogous Mukaiyama reactions leading to enantioenriched lactones **2** starting from silyldienolate **1**. Indeed, this methodology proved to be a powerful synthetic tool applied in the total synthesis of natural products (Scheme 1).[6,7]

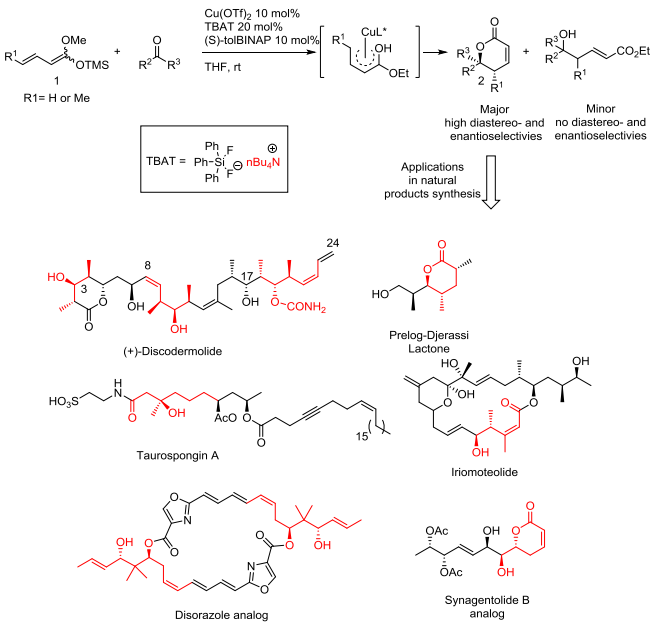

Scheme 1. Catalytic and asymmetric vinylogous Mukaiyama reactions for the synthesis of enantioenriched lactones **2** and applications in natural product synthesis.

The catalytic system ($Cu(OTf)_2$, (*S*)-tolBINAP, TBAT) used in these reactions was originally developed by Carreira in the first enantioselective vinylogous Mukaiyama reaction based on the activation of the cyclic silyl dienolate **3** (Scheme 2).[8,9]

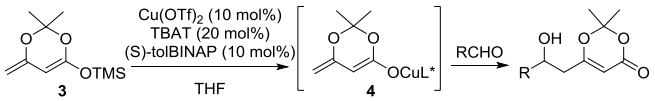

Scheme 2. Carreira's catalytic and asymmetric vinylogous Mukaiyama (CVAM) reaction.

An IR study by Carreira suggested the formation of a Cu(I) dienolate intermediate **4** as a possible reactive species but the exact structure of which was unknown (Scheme 2).[9]**Erreur ! Signet non défini.** In our own work[6] we used linear silyl dienolates **1a,b** that could give rise to a complex mixture of Cu(I) dienolate species **5**-**7** (Scheme 3). Therefore the reactivity could result from an allyl copper or a copper enolate reagent due to the possible metallotropic equilibria between O-metalated and C-metalated (α and γ) forms.[10]

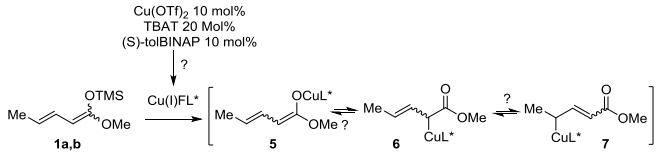

Scheme 3. Possible metallotropic equilibrium between *O*-metalated and *C*-metalated forms.

With the aim to understand the peculiarities of this transformation and to extend its synthetic scope, we were keen to unveil the mechanism of formation of the reactive species and to determine their real structures in solution. We thus undertook intertwined experimental, analytical and DFT studies in order to determine i) the nature of the precatalytic species formed from the catalytic system ($Cu(OTf)_2$, (*S)*-tolBINAP, TBAT) ii) the nature of the catalytic species obtained through reaction of these precatalytic species with silyl dienolate **1a,b**.

Results and Discussion

Determination of precatalytic species formed from the catalytic system:

Experimentally, the standard reaction conditions are: a solution of $Cu(OTf)_2$ (10 mol%) and (*S*)-tolBINAP (10 mol%) in anhydrous THF is stirred from 30 minutes at room temperature (rt, a clear yellow solution was obtained).[6c,f] A solution of ((*n*-$Bu_4N)Ph_3SiF_2$ (TBAT)**,** 20 mol%, 2 equivalents compared to copper) in anhydrous THF is then added and, after an additional 15 minutes at this temperature, a bright yellow solution is obtained. The mixture of silyl dienolates **1a,b** (71:29, 1.5 equivalent) is added dropwise (the solution turned red brown in color) followed by the aldehyde (1 equiv.) and the resulting mixture is stirred overnight at rt. Although the copper precatalytic species was initially described as a "CuF_2(tol-BINAP)" complex by Carreira,[8] further studies suggested the formation of a copper(I) complex "CuF(tolBINAP)". Based on Carreira's hypothesis, a possible Cu(II) to Cu(I) reduction pathway could imply the oxidative coupling of the enolate moiety or phosphine oxidation.[9] However this mechanistic scenario does not explain the need of two equivalents of TBAT per Cu(II) salt. Indeed, no product was formed when we performed the vinylogous Mukaiyama reaction in the presence of 1 equivalent of TBAT (table 1, compare entries 1 and 2). Interestingly, the reaction proceeds efficiently in the presence of 1 equivalent of TBAT using a Cu(I) salt ($Cu^{I}OTf)_2$ instead of $Cu^{II}(OTf)_2$ (table 1, entry 3). This result suggests that the TBAT could be implied in the reduction process and that in these reaction conditions BINAP is not able to reduce the Cu(II) salt at rt.[11]

Table 1. Influence of copper salts on the vinylogous Mukaiyama reaction leading to lactone **2a**

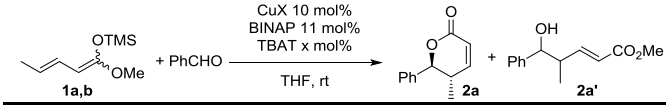

Entry	CuX	Copper/TBAT ratio	Conversion % [a]
1	$Cu^{II}(OTf)_2$	1:2	> 90%
2	$Cu^{II}(OTf)_2$	1:1	No reaction
3	$(Cu^{I}OTf)_2{\cdot}C_6H_6$	1:1	> 90%

[a] Based on silylated dienolate **1a** + **1b**

This hypothesis prompted us to undertake coupled NMR and cyclic voltammetry (CV) studies in order to monitor changes in copper complex leading to the formation of the precatalyst species. These analysis were sequentially carried out at three different stages; i) the 1:1 mixture of $Cu(OTf)_2$ and BINAP, then ii) the addition of one equivalent of TBAT and finally iii) the addition of a second equivalent of TBAT:

Stage 1: $Cu^{II}(OTf)_2$ + BINAP → C1
Stage 2: C1+ TBAT → C2
Stage 3: C2 + TBAT → C3

Our aim is thus to determine the nature of C1 to C3 complexes. Since the fluorine atom seems to be closely associated to the catalyst, NMR studies focused on this nucleus. The reaction conditions were thus reproduced in an NMR tube and monitored by ^{19}F NMR experiments, and CV studies were conducted simultaneously (Figure 1). Indeed CV is also a useful analytical technique to obtain mechanistic information, taking advantage that the oxidation or reduction currents are proportional to the concentration of electroactive species to examine directly the oxidation degree of the Cu atom. Furthermore, CV enables to study highly reactive species (*short-lived* species), as they appear stable at the time of the cyclic voltammetry.[12] The electrochemical behavior of Cu(I) or Cu(II) in the presence of chelating ligands is well documented, but generally with diimine ligand such as bipyridine or phenanthroline, and more specifically for the oxidation of Cu(I) to Cu(II).[13] Some papers reported organic phosphines as well as their bidentate derivatives as ligand of copper, but the majority of these studies deal with mixed-ligand complexes, those contain phenylphosphine only as spectator and the cathodic behavior of Cu(I) complexes generally shows a ligand-centered reduction, the Cu(0) formation being not visible.[14] Finally few works concerning copper BINAP complexes are reported,[15] and no on electrochemistry.

The overall results of stages 1 to 3 are reported in Figures 1 (NMR) and 2-4 (CV)

Stage 1 : $Cu(OTf)_2$ + BINAP

At first, the ^{19}F NMR spectra of $Cu^{II}(OTf)_2$ was recorded in anhydrous THF-d_8 at room temperature with increasing amounts of rac-BINAP (ie Cu:BINAP = 1:0.25; 1:0.5; 1:1). A broad signal at -54.0 ppm is observed for $Cu^{II}(OTf)_2$. The signal becomes thinner and is shielded as the amount of BINAP is increased. At a 1:1 ratio, a signal at -77.4 ppm is observed (See SI Figure E for details). Interestingly, no signal of 'free' $Cu^{II}(OTf)_2$ could be observed even for the use of sub-stoichiometric amount of BINAP, suggesting a rapid exchange between Cu(II) and BINAP (See SI Figure E). In a second set of experiments, CV were carried out on a 0.1 M solution of *n*-Bu_4NBF_4 used as supporting electrolyte in THF at room temperature. The electrochemical behavior of Cu(II) was studied at a scan rate of 500 $mV.s^{-1}$ by addition of $Cu^{II}(OTf)_2$ (10 mM). Initially, an irreversible reduction peak R_1 was detected at -0.05 V/SCE (see SI, Figure C). After addition of BINAP (10 mM), R_1 disappeared and a new reduction peak R_2 developed at -1.25 V/SCE (Figure 2a), attesting the complexation of Cu(II) by BINAP. This non-reversible signal, assigned to the reduction of Cu(II) into Cu(0), both coordinated to the ligand BINAP, is relatively large because of the presence of different complexes in equilibrium in solution that can be reduced at very close potentials. The presence of one equivalent of BINAP generates a new system R_3 at -2.1 V/SCE. This peak can be attributed to the reduction process of BINAP into BINAP$^{\cdot -}$ associated to Cu(0). It must be pointed out that BINAP was not found to be reducible in a separate experiment performed under the same conditions (See SI Figure D).

In order to compare Cu(II) and Cu(I), and thus to make sure that no reduction of Cu(II) had taken place through addition of BINAP, we have studied by CV the electrochemical behavior of $(Cu^{I}OTf)_2 \bullet C_6H_6$ in the presence of BINAP (Figure 2b) in the same experimental conditions. We note that the presence of BINAP leads to the disappearance of the reduction of Cu(I) at -0.35 V/SCE (see SI) and the emergence of a new electrochemical system at -1.04 V/SCE. If we compare the two curves obtained with Cu(I) and Cu(II), we can notice a few difference in the electrochemical behavior: the signal observed at -1.25 V/SCE in the case of "Cu(II)•BINAP" is shifted towards the less negative potentials (centered at -1.04 V/SCE) and is twice smaller, which is consistent with a one electron reduction compared to the two electron system involved with Cu(II). The peak at -2.1 V/SCE attributed to the reduction process of BINAP into BINAP$^{\cdot -}$ associated to zero-valent copper is still present.

Stage 2: Addition of the first equivalent of TBAT

The addition of one equivalent of TBAT in a solution containing "Cu(II)•BINAP" complex leads to the formation of a copper species that is reducible at -1.04 V/SCE that is similar to the reduction potential of "Cu(I)•BINAP" observed above (Figure 2b, Figure 3a-b and Figure 4). It is thus possible to assume that TBAT induces the reduction of "Cu(II)•BINAP" into "Cu(I)•BINAP".

The ^{19}F NMR spectra of the 1:1 mixture of $Cu(OTf)_2$•BINAP and TBAT shows a lack of a broad peak at -77 ppm and the appearance of two new peaks at -78 and -170 ppm. The first one was attributed to the overlay of the OTf signals in *n*-Bu_4NOTf and in $Cu^{I}OTf$•BINAP. Indeed the comparison of the ^{19}F NMR spectra of *n*Bu_4NOTf (generated from TBAF and TMSOTf), and the copper salt obtained by the mixture of one equivalent of $(Cu^{I}OTf)_2 \bullet C_6H_6$ with two equivalents of BINAP shows that these two species have the same chemical shift (See SI). The second one was attributed to Ph_3SiF by comparison with an authentic sample (See SI).

Stage 3: Addition of the second equivalent of TBAT

When one more equivalent of TBAT is added to the 1:1:1 mixture of $Cu^{II}(OTf)_2$, BINAP and TBAT, the "$Cu^{I}OTf$•BINAP" ^{19}F NMR signal disappear and a new signal can be observed at -138 ppm. This signal was attributed to "CuF•BINAP".[16] Indeed, when mixing half an equivalent of $(Cu^{I}OTf)_2 \bullet C_6H_6$ complex with one equivalents of BINAP and one equivalent of TBAT, the same signal could be observed at -138 ppm (along with Ph_3SiF and *n*-Bu_4NOTf signals, see SI).

This point was also examined through CV. After addition of a second equivalent of TBAT, the reduction peak of Cu(I) at -1.04 V/SCE disappeared totally, and a new reversible system appeared at -1.9 V/SCE (Figure 3c). This was also observed when introducing only one equivalent of TBAT in a "Cu(I)•BINAP" solution. According to these observations, this new system can be attributed to the reduction of the "CuF•BINAP" complex, which is the precatalyst during the CAVM process. These characteristic reduction steps are summarized in Scheme 4.

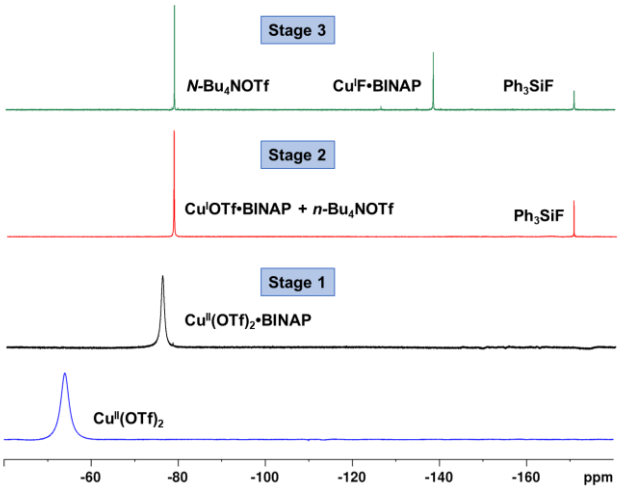

Figure 1. ^{19}F NMR spectra (470 MHz, THF-d_8, 298K) of solution of: (1) $Cu(OTf)_2$ (blue spectrum); (2) $Cu(OTf)_2$ +BINAP (black spectrum); (3) $Cu(OTf)_2$ +BINAP + 1eq TBAT (red spectrum) (4) $Cu(OTf)_2$ +BINAP + 2eq TBAT (green spectrum)

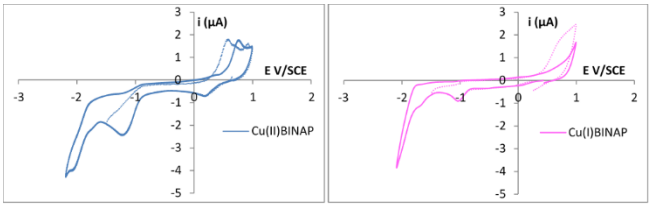

Figure 2. Cyclic Voltammograms in THF + 0.1 M NBu_4BF_4, at a gold disc microelectrode (0.25 mm diameter) at v = 0.5 $V.s^{-1}$ and at r.t. **Figure 2a**- 10^{-2} M $Cu(OTf)_2$ + 1 molar equiv. of BINAP (blue curve); **Figure 2b**- 10^{-2} M CuOTf + 1 molar equiv. of BINAP (pink curve)

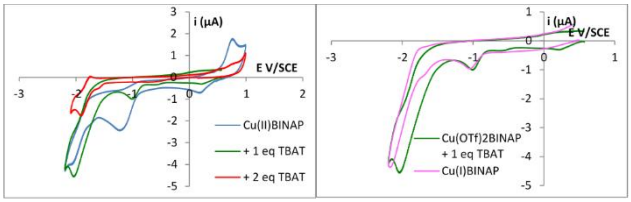

Figure 3. Cyclic Voltammograms in THF + 0.1 M NBu_4BF_4, at a gold disc microelectrode (0.25 mm diameter) at v = 0.5 $V.s^{-1}$ and at r.t. a- 10^{-2} M $Cu(OTf)_2$ + 1 molar equiv. of BINAP (blue curve); b- + 1 molar equiv. TBAT (green curve); c- + 2 molar equiv. TBAT (red curve).

Figure 4. Cyclic Voltammograms in THF + 0.1 M NBu_4BF_4, at a gold disc microelectrode (0.25 mm diameter) at v = 0.5 $V.s^{-1}$ and at r.t. a- 10^{-2} M $Cu(OTf)_2$ + 1 molar equiv. of BINAP + 1 molar equiv. TBAT (green curve); b- 10^{-2} M CuOTf + 1 molar equiv. of BINAP (pink curve).

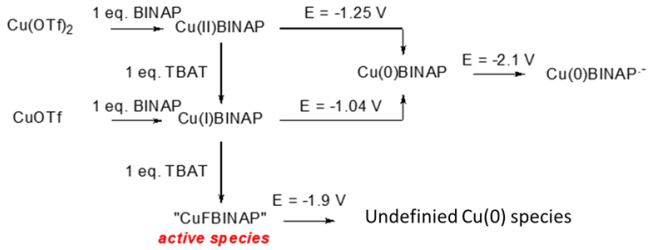

Scheme 4. Reduction of Cu(I) and (II) in presence of BINAP and TBAT.

The above observations (experimental, ^{19}F NMR and CV) are in good accordance with Carreira's hypothesis of "CuF•tolBINAP" as the relevant precatalyst.[9] Furthermore, all these experimental evidences show that TBAT (2 equivalents per copper) has two distinct roles: the reduction of Cu(II) in Cu(I) and the formation of the active "CuF•diphosphine" precatalyst.

Nature of the catalytic species obtained through reaction of these precatalytic species with silyldienolates.

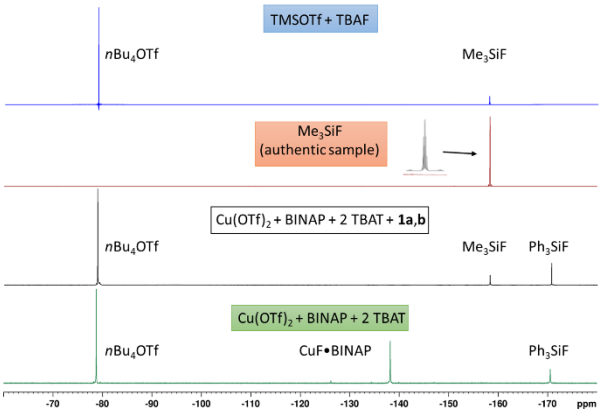

Figure 5. Study of the formation of the Cu^{I} dienolate reagent: ^{19}F NMR spectra (470 MHz, THF-d_8, 298K) of mixture of (1) $Cu(OTf)_2$ +BINAP+ 2TBAT (green spectrum); (2) $Cu(OTf)_2$ + BINAP + 2TBAT + **1a,b** (black spectrum); (3) Me_3SiF (red spectrum) and (4) TMSOTf + TBAT (bleu spectrum).

The next step of our study deals with the reactivity of the above identified precatalyst with the silyldienolates **1a,b** (see Scheme 3). This study was carried coupling multinuclear NMR studies and computational investigations.

When the 71:29 *E*:*Z* mixture of silyldienolates **1a,b** was added to the $Cu^{II}(OTf)_2$ / BINAP / TBAT (2 equiv) mixture, the -138 ppm signal disappeared with the concomitant apparition of a signal at -158 ppm that corresponds to TMSF (attributed by comparison with an authentic sample, see Figure 5). As previously suggested by control experimental results (see table 1 and stage 2) this confirm that the Cu(II) complex is reduced to Cu(I) in the presence of TBAT. This can be associated to a dienolate chain transfer step to the Cu(I), associated to an exchange with F and thus further confirms that the -138 ppm signal corresponds to a "CuF" species.

Table 2. Energies / Gibbs Free energy with respect to the most stable silyldienolate **SE** (s-trans) in kcal mol^{-1}

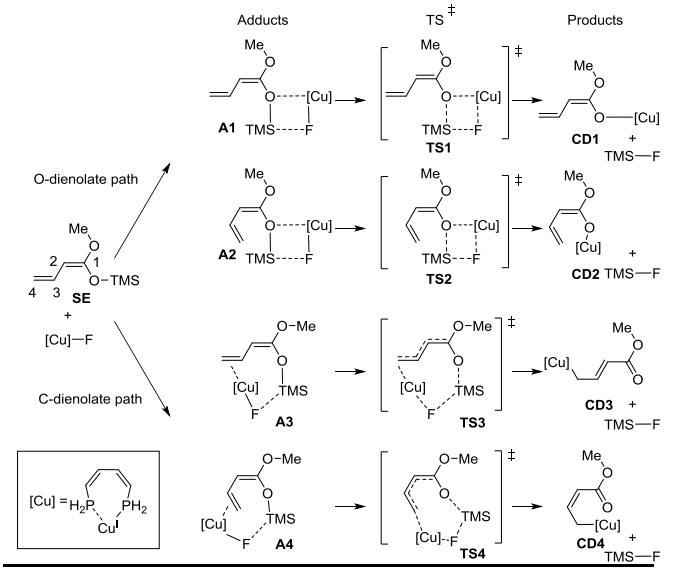

Entry	Adduct	TS	Products	
1	**A1**: -8.3 / 3.4	**TS1**: -0.4 / 13.8	Cu-O-dienolate s-*trans* **CD1**	-12.4 / -12.2
2	**A2**: -6.1 / 6.3	**TS2**: 1.0 / 15.1	Cu-O-dienolate s-*cis* **CD2**	-18.0 / -17.9
3	**A3**: -12.1 / 1.2	**TS3**: -1.2 / 13.4	Cu-C-dienolate s-*trans* **CD3**	-17.6 / -16.3
4	**A4**: -8.9 / 4.9	**TS4**: -2.1 / 13.1	Cu-C-dienolate s-*cis* **CD4**	-18.0 / -17.8

This TMS/F exchange step has extensively been studied computationally by some of us recently, using $[Cu(PH_3)_2]^+$ as a model copper complex.[17] We demonstrated that the exchange between F and a highly conjugated enolate chain like the one used here is highly exergonic and irreversible. The same mechanism was recomputed here, using a "small model" of the Cu(I)•tolBINAP to replace the Cu(I)•$(PH_3)_2$ complex used previously (see computational details) and a non-substituted silyl dienolate **SE** (see Table 2).[18] Similar results are obtained, with a Gibbs free energy of activation of 13.8 kcal mol^{-1} for enolate / F exchange (**TS1**) and an exergonicity of 12.2 kcal mol^{-1} (**P1**).

Nevertheless, an additional reaction path could be located, that takes advantage of the formation of π-adduct **A3** and **A4** between the [Cu]-F precatalytic species and the terminal C=C double bond to directly yield C-bonded copper dienolates **CD3**.[19] Reaction pathways yielding to Cu-C- and Cu-O-dienolates both in s-*cis* and s-*trans* arrangement around the C_2-C_3 bond **CD1**-**4** were localized, and their Gibbs free energy data are gathered in Table 2. Although we had expected significant differences, it appears that all pathways are close in energy. Whatever the pathway at stake, these results confirm that the precatalyst is converted in an irreversible manner to a copper dienolate complex **P1**-**4** in presence of the silyldienolate **SE**.

The structure determination of these various Cu-dienolate reagents **CD1**-**4** was next attempted using NMR {^{1}H, ^{13}C} spectroscopy. However, in the real reaction conditions (10 mol% of copper), the organocopper species are obtained in a too small concentration to enable their direct observation. The structures were thus sampled more closely through DFT computations.

.

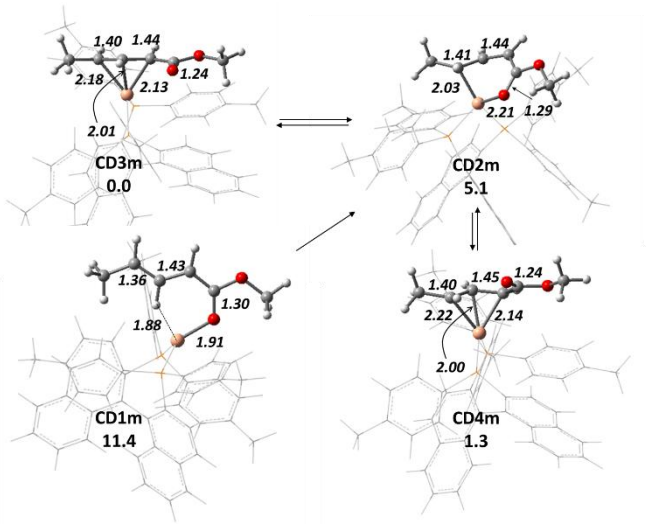

Figure 6. The four most stable optimized Cu-dienolate. Energies of the minima are given (below structures) in kcal mol^{-1} with respect to the most stable isomer. Distances (in italic) are given in Å.

The computational studies were first carried out using the simplified model described in table 2. More than 20 different structures could be obtained, depending on conformations and side coordination. The obtained structures can be classified among four categories analogous to the Cu dienolates products described in Table 2 that mainly differ by the s-*cis* or s-*trans* conformation of the ester moiety.[20] The most stable structures in each category were then recomputed using a complete model including the full tolBINAP ligand and the γ-substituted copper dienolate. They correspond to two Cu-O enolates (**CD1m** and **CD2m**) and two Cu-C enolates (**CD3m** and **CD4m**). The three most stable structures **CD2m-4m** shown in Figure 6 all lie within 5 kcal mol^{-1}. The *trans* dienolate are found in Cu-O and Cu-C form, but the Cu-O structure **CD1m** is high in energy compared to **CD2m**-**4m**. The C-copper dienolates **CD3m** and **CD4m** exhibit a η^3 terminal coordination, whatever the s-*trans* or s-*cis* conformation of the chain. In both cases, the Cu…O=C(OMe) distance is above 3 Å and can be considered as non-bonding. Finally, the O-copper *cis*-dienolate **CD2m** is best described as a dicoordinated (κ^2 coordination) through both C and O, due to the interaction of the terminal carbon with copper (Cu-C = 2.03Å), which is enabled by the *cis* configuration. The **CD3m** and **CD4m** complexes are found to be in equilibrium through **CD2m** (see supplementary information for equilibration TS), and **CD1m** is too high in energy to be in significant proportion in the medium, and can easily interconvert to **CD4m** (see supplementary information for interconversion barriers and transition states structures).

Behavior of the solution of Cu-dienolate in catalytic conditions

The reaction was next conducted in a NMR tube using the mixture of silyldienolate **1a** and **1b** and a catalytic amount of the precatalyst [Cu]F, and was monitored by 2D ^{1}H and ^{13}C NMR spectroscopy (See SI). Even though the organocopper reagent generated was in too low concentration to be directly observed using this procedure, we had interesting NMR results concerning the behavior of the silyldienolates precursor **1a,b**. Indeed, the silyldienolates **1a,b** were characterized by 1D ^{1}H and 2D ^{1}H NOESY NMR experiments (See SI) as a well-defined 71:29 mixture of two *E*/*Z* diastereoisomers. When reacted in presence of catalytic amount of the Cu(BINAP)F precatalyst, a much more complex mixture of silyldienolates was obtained, and at least 5 different forms could be detected in the reaction medium (See SI). Among them, the initially major form **1a** had nearly totally disappeared (from 71 to 4%), the amount of the formerly minor isomer **1b** had significantly increased (from 29 to 57%), whereas new structures **1c**, **1d** and **1e** appeared (Scheme 5).

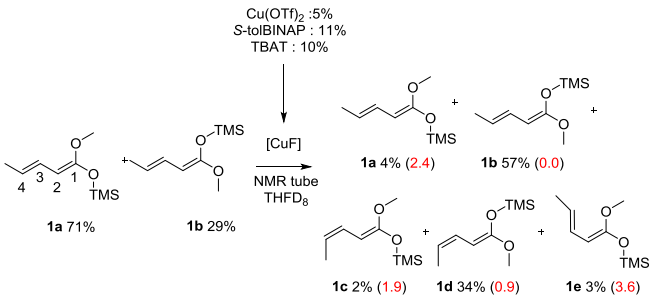

Scheme 5. Respective fractions of the silyldienolate isomers observed by NMR and energies (kcal mol^{-1}) relative to the most stable isomer **1b** (in red in parenthesis).

Computational evaluation of the relative stabilities of these silyl dienolate isomers reveals that the abundance of isomers **1a-d** in presence of the precatalyst experimentally determined by NMR studies fits closely to their computed relative stabilities. The two most abundant (**1b** and **1d**) are by far the most stable whereas **1a**, **1c** and **1e** are more than 1.9 kcal mol^{-1} higher in energy.

The observation of silyl dienolates **1a-e** underscores an unexpected and spectacular conformational and stereochemical scrambling around the two double bonds of the starting mixture of silyl dienolates **1a,b**. The formation of compounds **1c** and **1d** highlights a *E*→*Z* isomerization of the C3=C4 double bond, and compound **1e** results from a s-*trans* to s-*cis* conformational

change in the **1a** ↔ **1e** equilibrium. Whereas the **1a** to **1e** equilibrium is a simple conformational change, the increase in the amount of **1b** and the appearance of structures **1c** and **1d** evidence the isomerization of both the C3=C4 (**1c** and **1d** formation) and the C1=C2 (**1b** growing from 29 to 57%) double bonds. Considering that these *E*/*Z* isomerization's are not observed in absence of the catalytic system, it can be proposed that the equilibration process takes place in the Cu-C-enolate complex, whose bonds exhibit a significant single-bond character (Scheme 6).

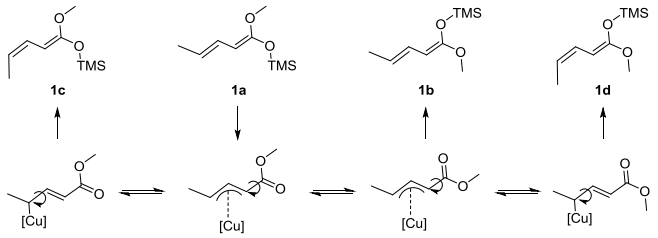

Scheme 6. Equilibration of the silyldienolate 1a-d through a copper η^1-η^3 coordination exchange.

The observed conformational/stereochemical scrambling of the double bonds is in full line with experimental results obtained starting from silyl dienolate isomers.[6f] Starting either from silyl dienolate **7** with a C3=C4 double bond of *E* configuration (obtained from the conjugated ester **9**) or from the corresponding C3=C4 *Z* double bond isomer **8** (obtained from the deconjugated ester **10**), the same lactone **2a** was obtained with similar yields, diastereo- and enantioselectivities. Same observations could be drawn from the reactions yielding the lactone **2b** starting from silyl dienolates **11** and **12** obtained in either 40:60 or 90:10 C1=C2 *Z*/*E* mixtures (Scheme 7).

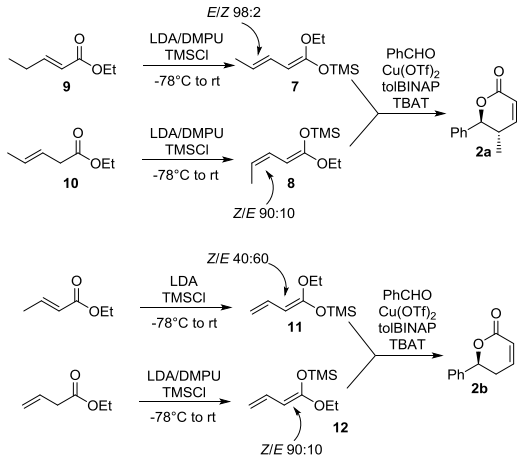

Scheme 7. Observed stereoconvergence in the formation of lactones **2a** and **2b** starting from the corresponding silyldienolates isomers **7**, **8**, **11** and **12**.

Equilibration between the silyl dienolate thus requires reversible chain exchange between Cu-enolate and silyldienolate, which cannot be confirmed experimentally as no Cu-enolate could be observed. The chain exchange process was thus examined computationally in a similar approach than for the case of the *trans* O-dienolate pathway described above, replacing F by dienolate (see Table 2). The obtained TS is significantly higher than the one obtained for the F/dienolate exchange. It is nevertheless small enough to justify equilibration between Cu- and Si-dienolate (Scheme 8).

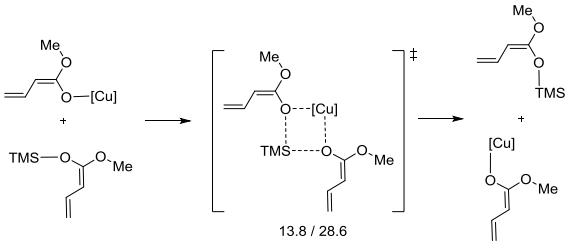

Scheme 8. O-dienolate pathway for identity dienolate chain Cu/Si exchange. The Energy / Gibbs free energy of the TS is given below its schematic representation in kcal/mol

Conclusion

Through coupling of synthetic, NMR, electrochemical and DFT studies, we have been able to determine the nature and the formation pathway of the catalytic system in Mukaiyama reaction. The TBAT is shown to play the role of reducing and fluorinating agent, resulting in a CuF(tolBINAP) precatalyst. The catalytic active species is proposed to be the Cu-dienolate species resulting from F/dienolate chain exchange between Cu(tolBINAP) and $SiMe_3$. This species was characterized computationally and both Cu-C and Cu-O dienolate structures are described. Nevertheless, the three quasi-isoenergetic structures described all exhibit a short Cu-C distance, and either an η^3-terminal coordination or a κ^2(C,O) bonding. This highlights the importance of the Cu-C interaction in shifting the metallotropic equilibrium toward its formation. In catalytic conditions, this Cu-dienolate complex is found to carry out slow equilibration with the remaining silyldienolate and to undergo rapid isomerization along all the dienolate chain. This is the sign of a fast metallotropic equilibrium within the Cu-dienolate. These findings are the starting point for the determination of reaction mechanisms for which Cu-dienolates are reaction intermediates in the presence of electrophiles.

Experimental Section

Computational details: Computations were undertaken using a simplified chelating disphosphine ligand instead of BINAP, resulting upon coordination to Cu^+ as shown in the complex in Figure A. This simple model allowed to sample a large number of structural arrangements, and to an extend study of the Cu/Si exchange pathways.

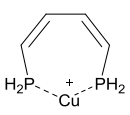

Figure A. Simplified model for Cu(tol-BINAP).

Full geometry optimizations were systematically conducted with no symmetry restraints using the Gaussian 09 program[21] within the framework of the Density Functional Theory (DFT) using the PW91 exchange-correlation functional[22] and the 6-31++G** basis set for all atoms as implemented in the Gaussian program. In the case of the calculation on the complete tolBINAP ligand, the 6-31G** is used. In the case of the sillyldienolate **1a** to **1e**, the B3PW91 functional[23] associated to Grimme's Empirical Dispersion (D3 version with Becke-Johnson damping BJ)[24] are used, to include dispersion effects in the relative stability of all isomers. Solvation effects are also included using the SMD model,[25] in the standard implementation in Gaussian, using THF as a solvent. The electronic plus nuclear energy obtained from SCF and optimization procedures is referred as energy and noted E in the text. Frequencies were evaluated within the harmonic approximation and used unscaled to compute Gibbs free energy (G) at 298.15 K using the standard protocol implemented in Gaussian.

Experimental details:

General Considerations: Experiments were carried out under dry argon atmosphere. All glassware were dried at 120°C and assembled while hot under a stream of argon. All moisture-sensitive reactants are handled under a nitrogen atmosphere. Low temperature experiments are carried out by cooling down a three-necked round bottom flask with an ether/acetone (-80/-90 °C), bath, frozen with liquid nitrogen. The flask was equipped with an internal thermometer, an argon inlet and a septum cap. Tetrahydrofuran was distilled from sodium-benzophenone ketyl. Copper salts and MeONa were purchased from Aldrich, kept under argon atmosphere, and dried over P_2O_5 before use. IR data were recorded on a Perkin Elmer Spectrum 1000 instrument. ^{1}H NMR spectra were recorded at 500 MHz or 300 MHz, ^{13}C NMR spectra were recorded at 125 MHz or 75 MHz, ^{29}Si spectra were recorded at 99 MHz and ^{19}F NMR spectra were recorded at 470 MHz, in THF-d_8 or $CDCl_3$ as solvent on Bruker Ultra Shield 500 or 300 spectrometers. Chemical shifts are reported in ppm.

Synthesis of (3*E*,1*Z*)-(1-Methoxypenta-1,3-dienyloxy)trimethylsilane 1a,b: *n*-BuLi (7 mL, 11 mmol) was added dropwise to a solution of N,N'-diisopropylamine (DIPA; 1.5 mL, 11 mmol) in anhydrous THF (20 mL) at -50 °C. The mixture was stirred for 30 min, cooled to -78 °C. The resulting solution was stirred for 30 min and then (*E*)-methyl pent-3-enoate ester (1.23 mL, 10 mmol) was added. This mixture was stirred for 30 min and then a solution of trimethylsilane chloride (TMSCl; 2 mL) in anhydrous THF (2 mL) was added over a period of 15 min. The resulting solution was allowed to warm to room temperature and stirred for 2 h. The solvent was removed under reduced pressure, the residue was taken up in pentane (50 mL), and this solution was filtered off. The solvent was removed under reduced pressure and the crude material was distilled in a Kugelrohr apparatus (45 °C, 1 mmHg) to furnish the desired silyl dienolate as an inseparable mixture. (1 *Z*/*E* 71:29, 3 *E*/*Z* > 98:2). For the major product: ^{1}H NMR (300 MHz, $CDCl_3$, 25°C): 6.10 ppm (m, 1 H), 5.33 (dq, 1H, *J* =14.9, 6.9 Hz), 4.41 (d, 1H, *J* = 10.3 Hz), 3.56 (s, 3 H), 1.72 (dd, 3H, *J* = 1.4, 6.9 Hz), 0.23 (s, 9H). These data are in accordance with those reported in literature.[6f] ^{1}H NMR (500 MHz, THF-*d8*, 25°C): 6.15 (m, 1H), 5.24 (m, 1H), 4.46 (m, 1H), 3.56 (s, 3H), 1.71 (dd, 3H, *J* = 1, 6.5 Hz), 0.29 (s, 9H). ^{13}C NMR (125 MHz, THF-*d8*, 25°C): 154.5, 127, 88.1, 54.9, 18.4, -0.28. ^{29}Si (99MHz, THF-*d8*, 25°C): 20.2 (s, 1Si).

Electrochemical measurements details: An SP-300 BioLogic apparatus was used for electrochemical experiments. They were carried out at room temperature, under an argon atmosphere, in a three-electrode cell containing tetrahydrofuran (THF, 10 mL) as solvent and tetrabutylammonium tetrafluroborate ($TBABF_4$, 10^{-1} mol.L^{-1}) as supporting salt. The reference electrode was a saturated Hg/Hg_2Cl_2 reference electrode (noted SCE for Saturated Calomel Electrode) from Tacussel. It was separated from the cell solution by a bridge compartment filled with the same solvent / supporting electrolyte solution as used in the cell. The counter electrode was a platinum wire. The working electrode was a disk obtained from a cross-section of a gold wire (d = 250 μm) sealed in glass.

Acknowledgements

The authors thank CCR (Univ. Paris VI, Paris, France), CINES (Montpellier, France), IDRIS (Orsay, France) and CRIHAN (Rouen, France) for computing facilities, and Clariant and the programme franco-algérien de formation supérieure and ANR Copenol (Projet ANR-09-BLAN-0089) for financial support.

Keywords: Silyl dienolate • copper dienolate • Ab initio calculations • Structure elucidation • Reaction mechanisms

[1] (a) J. Deschamp, O. Chuzel, J. Hannedouche, O. Riant, *Angew. Chemie - Int. Ed.*, 2006, **45**, 1292–1297. (b) H. W. Lam, P. M. Joensuu, *Org. Lett.* **2005**, *7*, 4225-4228. (c) J. Deschamp, T. Hermant, O. Riant, *Tetrahedron*, **2012**, *68*, 3457–3467. (d) J. Deschamp, T. Hermant, O. Riant, *Tetrahedron*, **2012**, *68*, 3457–3467. (e) D. Zhao, K. Oisaki, M. Kanai, M. Shibasaki, *Tetrahedron Lett.*, **2006**, ***47***, 1403–1407. (f) J. Deschamp, O. Riant, *Org. Lett.*, **2009**, *11*, 1217–1220. (g) J. Ou, W. T. Wong, P. Chiu, *Org. Biomol. Chem.* **2012**, *10*, 5971–5978.

[2] (a) K. Oisaki, Y. Suto, M. Kanai, M. Shibasaki, *J. Am. Chem. Soc.* **2003**, *125*, 5644–5645. (b) K. Oisaki, D. Zhao, Y. Suto, M. Kanai, M. Shibasaki, *Tetrahedron Lett.* **2005**, *46*, 4325–4329. (c) K. Oisaki, D. Zhao, M. Kanai, M. Shibasaki, *J. Am. Chem. Soc.* **2006**, *128*, 7164–7165. (d) [1] Y. Suto, M. Kanai, M. Shibasaki, *J. Am. Chem. Soc.* **2007**, *129*, 500–501.

[3] K. Oisaki, D. Zhao, M. Kanai, M. Shibasaki, *J. Am. Chem. Soc.* **2007**, *129*, 7439–7443.

[4] (a) A. R. Burns, J. Solana González, H. W. Lam, *Angew. Chemie - Int. Ed.* **2012**, *51*, 10827–10831. (b) Q. Zhang, X. Jia, L. Yin, *Tetrahedron* **2019**, *75*, 1676–1681.

[5] (a) H. J. Zhang, L. Yin, *J. Am. Chem. Soc.* **2018**, *140*, 12270–12279. (b) F. Zhong, W. J. Yue, H. J. Zhang, C. Y. Zhang, L. Yin, *J. Am. Chem. Soc.* **2018**, *140*, 15170–15175. (c) H. J. Zhang, C. Y. Shi, F. Zhong, L. Yin, *J. Am. Chem. Soc.* **2017**, *139*, 2196–2199. (d) M. Zhang, N. Kumagai, M. Shibasaki, *Chem - Eur. J.* **2016**, *22*, 5525-5529. (e) S. Wang, Z. Liu, W. Yue, L. Yin, *Angew. Chemie* **2021**, *60*, 1–6.

[6] (a) G. Bluet, J. M. Campagne, *Tetrahedron Lett.* **1999**, *40*, 5507–5509. (b) G. Bluet, J.-M. Campagne, *Synlett* **2000**, 221-222. (c) G. Bluet, B. Bazán-Tejeda, J.-M. Campagne, *Org. Lett.* **2001**, *3*, 3807-3810. (d) B. Bazán-Tejeda, M. Georgy, J.-M. Campagne, *Synlett* **2004**, 720-722. (e) X. Moreau, B. Bazán-Tejeda, J.-M. Campagne, *J. Am. Chem. Soc.* **2005**, *127*, 7288-7289. (f) B. Bazan-Tejeda, G. Bluet, G. Broustal, J.-M. Campagne, *Chem. - A Eur. J.* **2006**, *12*, 8358–8366. (g) K. Spielmann, R. M. De Figueiredo, J.-M. Campagne, *J. Org. Chem.* **2017**, *82*, 4737–4743.

[7] (a) G. Kumaraswamy, N. Raghu, N. Jayaprakash, K. Ankamma, *Tetrahedron* **2015**, *71*, 5472–5477. (b) R. Schäckel, B. Hinkelmann, F. Sasse, M. Kalesse, *Angew. Chemie Int Ed.* **2010**, *49*, 1619–1622. (c) L. Fang, H. Xue, J. Yang, *Org. Lett.* **2008**, *10*, 4645–4648. (d) K. Sato, M. Isoda, A. Tarui, M. Omote, *Eur. J. Org. Chem.* **2020**, *2020*, 6503–6511.

[8] J. Krüger, E. M. Carreira, *J. Am. Chem. Soc.* **1998**, *120*, 837–838.

[9] B. L. Pagenkopf, J. Krüger, A. Stojanovic, E. M. Carreira, *Angew. Chemie - Int. Ed.* **1998**, *37*, 3124–3126.

[10] (a) E. Vrancken, J.-M. Campagne, P. Mangeney in *Comprehensive Organic Synthesis 2nd edition, Vol 1* (Eds Gary A. Molander, Paul Knochel) (Eds.:), Oxford: Elsevier; 2014. pp. 74–123. (b) R. Y. Liu, Y. Zhou, Y. Yang, S. L. Buchwald, *J. Am. Chem. Soc.* **2019**, *141*, 2251–2256. (c) C. Li, R. Y. Liu, L. T. Jesikiewicz, Y. Yang, P. Liu, S. L. Buchwald, *J. Am. Chem. Soc.* **2019**, *141*, 5062–5070. (d) E. Y. Tsai, R.

Y. Liu, Y. Yang, S. L. Buchwald, *J. Am. Chem. Soc.* **2018**, *140*, 2007–2011. (e) R. K. Acharyya, S. Kim, Y. Park, J. T. Han, J. Yun, *Org. Lett.* **2020**, *22*, 7897–7902. (f) G. Xu, B. Fu, H. Zhao, Y. Li, G. Zhang, Y. Wang, T. Xiong, Q. Zhang, *Chem. Sci.* **2019**, *10*, 1802–1806. (g) X. W. Chen, L. Zhu, Y. Y. Gui, K. Jing, Y. X. Jiang, Z. Y. Bo, Y. Lan, J. Li, D. G. Yu, *J. Am. Chem. Soc.* **2019**, *141*, 18825–18835. (h) X. F. Wei, T. Wakaki, T. Itoh, H. L. Li, T. Yoshimura, A. Miyazaki, K. Oisaki, M. Hatanaka, Y. Shimizu, M. Kanai, *Chem* **2019**, *5*, 585–599.

[11] (a) F. H. Jardine, L. Rule, A. G. Vohra, *J. Chem. Soc. (A)* **1970**, 288. (b) Y. Kobayashi, T. Taguchi, T. Morikwa, E. Tokuno, S. Sekiguchi, *Chem. Pharm. Bull.* **1980**, *28*, 262–267. (c) D. Ferraris, B. Young, C. Cox, W. J. Drury, T. Dudding, T. Lectka, *J. Org. Chem.* **1998**, *63*, 6090–6091. (d) S. Nieto, P. Metola, V. M. Lynch, E. V. Anslyn, *Organometallics* **2008**, *27*, 3608–3610.

[12] (a) *Electrochemical Methods: Fundamentals and Applications 2nd ed* (Eds.: A. J. Bard, L. R. Faulkner), Wiley, **2000**, pp 12–18. (b) M. Durandetti, M. Devaud, J. Périchon, *New J. Chem.*, **1996**, *20*, 659-667. (c) O. Buriez, M. Durandetti, J. Périchon, *J. Electroanal. Chem.* **2005**, *578*, 63–70. (d) O. Buriez, M. Durandetti, J. Périchon, *J. Electroanal. Chem.* **2005**, *578*, 63–70. (e) A. Jutand, *Chem. Rev.* **2008**, *108*, 2300–2347.

[13] (a) D. Saravanabharathi, M. Nethaji, A. G. Samuelson, *Polyhedron* **2002**, *21*, 2793–2800. (b) K. Noda, T. Sasaki, S. Iwatsuki, K. Kashiwabara, T. Suzuki, H. D. Takagi, **2004**, *357*, 526–532. (c) R. Balamurugan, M. Palaniandavar, M. A. Halcrow, *Polyhedron* **2006**, *25*, 1077–1088.

[14] (a) O. Moudam, A. Kaeser, B. Delavaux-Nicot, C. Duhayon, M. Holler, G. Accorsi, N. Armaroli, I. Séguy, J. Navarro, P. Destruel, et al., *Chem. Commun.* **2007**, *3092*, 3077–3079. (b) E. Leoni, J. Mohanraj, M. Holler, M. Mohankumar, I. Nierengarten, F. Monti, A. Sournia-Saquet, B. Delavaux-Nicot, Jean-Francois Nierengarten, N. Armaroli, *Inorg. Chem.* **2018**, *57*, 15537–15549. (c) R. Giereth, A. K. Mengele, W. Frey, M. Kloß, A. Steffen, M. Karnahl, S. Tschierlei, *Chem. - A Eur. J.* **2020**, *26*, 2675–2684.

[15] (a) H. Kunkely, V. Pawlowski, A. Vogler, *Inorg. Chem. Commun.* **2008**, *11*, 1003–1005. (b) [1] X. Zarate, E. Schott, R. Ramirez-Tagle, D. MacLeod-Carey, R. Arratia-Pérez, *Polyhedron* **2012**, *37*, 54–59.

[16] (a) C. Rasson, O. Riant, *Org. Process Res. Dev.* **2020**, *24*, 835–840. (b) C. Rasson, A. Stouse, A. Boreux, V. Cirriez, O. Riant, *Chem. - A Eur. J.* **2018**, *24*, 9234–9237. (c) L. Cornelissen, V. Cirriez, S. Vercruysse, O. Riant, *Chem. Commun.* **2014**, *50*, 8018–8020. (d) D. J. Gulliver, W. Levason, M. Webster, *Inorg. Chim. Acta* **1981**, *52*, 153–159.

[17] S. Bouaouli, K. Spielmann, E. Vrancken, J.-M. Campagne, H. Gérard, *Chem. - A Eur. J.* **2018**, *24*, 6617-6624.

[18] The validation of the 'small model' to calculate the transition state of the TMS/F exchange relies on the comparison of energies of intermediates CD1m-CD4m respectively obtained with the 'small' and the 'full' model (see Figure 6 and SI, computation details section 3). As only slight differences could be observed in these energies, the small model was thus chosen to compute this TMS/F exchange barrier. Indeed, only a semi-quantitative assessment of the activation barrier is necessary to complement our previous mechanistic studie (ref 17) and confirms that the TMS/F exchange is not kinetically hampered.

[19] As **CD2** already exhibits some Cu…C interaction due to the S-cis configuration of the silyldienolate chain, **CD4** and **CD2** are quasi identical.

[20] Apart from this conformational difference, products with similar features are obtained. See supplementary information for comparison of structures.

[21] Gaussian 09, Revision .02D.01, Frisch, M. J. et al. Gaussian, Inc., Wallingford CT, 20042013.

[22] J. P. Perdew, K. Burke, Y. Wang, *Phys. Rev. B* **1996**, *54*, 16533-16539. And ref. therein

[23] A. D. Becke, *J. Chem. Phys.* **1993**, *98*, 5648-5652.

[24] S. Grimme, S. Ehrlich, L. Goerigk, *J. Comp. Chem.* **2011**, *32*, 1456-65.

[25] A. V. Marenich, C. J. Cramer, D. G. Truhlar, *J. Phys. Chem. B* **2009,** *113*, 6378-96.

Entry for the Table of Contents

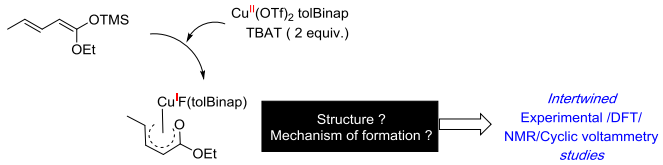

An intertwined analytical, experimental and theoretical study disclose the mechanism of formation of an organocopper dienolate reagent from its silylated precursor. The study shed light on thee Cu(II) to Cu(I) reduction process, the Si to Cu exchange mechanism and finally the metallotropic equilibrium of the resulting copper dienolate.